Astronomy & Astrophysics manuscript no. ccingles2bbb˙mgr160206 April 20, 2006
(DOI: will be inserted by hand later)

Hα line profiles for a sample of supergiant HII regions

II. Broad, low intensity components

M. Rozas,[1] M.G. Richer,[1] J.A. López,[1] M. Relaño,[2] J.E. Beckman[3]

[1] Instituto de Astronomía, Universidad Nacional Autónoma de México, Ensenada, México
e-mail: maite@astrosen.unam.mx
[2] Facultad de Ciencias. Universidad de Granada. Spain
e-mail: mrelano@ugr.es
[3] Instituto de Astrof´ isica de Canarias, La Laguna, Tenerife, Spain
e-mail: jeb@ll.iac.es

the date of receipt and acceptance should be inserted later

Abstract. We analyze the broad, low intensity, high velocity components that are seen in the Hα line profiles for a sample of HII regions. These HII regions are chosen from among the brightest and most isolated in a sample of spiral galaxies for which we have photometric and spectroscopic data: NGC 157, NGC 3631, NGC 6764, NGC 3344, NGC 4321, NGC 5364, NGC 5055, NGC 5985, and NGC 7479. We confirm that the line profiles of most of these bright, giant extragalactic HII regions contain broad kinematic components of low intensity, but high velocity, that we denote as wings. We analyze these components, deriving emission measures, central velocities, and velocity dispersions of the blue and red features, which are similar. We interpret these components as expanding shells within the HII regions and produced by the stellar winds from the ionizing stars. We compare the kinetic energies of these expanding shells with the kinetic energy available from the stellar winds. If we allow for the hypothesis that the brightest HII regions are density bounded, we show that, for these HII regions, the stellar wind mechanism can explain the observed shell kinetic energies.

Key words. ISM: HII regions – ISM: kinematics and dynamics –

1. Introduction

The kinematics of the gas in HII regions may be studied through the profiles of the emission lines in HII regions. A variety of line profile studies have found broad, low intensity components with high velocities in giant extragalactic HII regions, but the interpretation of these kinematic components is complicated due to the high velocities, low densities, and large sizes of the emitting regions (Arsenault & Roy 1986; Castañeda, Vilchez & Copetti 1990, Peimbert, Sarmiento & Fierro 1991, Kennicutt 1994; Yang et al. 1996; Chu & Kennicutt 1994; Rosa & Solf 1984; Sabalisck et al. 1995, Izotov et al. 1996). The most fruitful efforts so far attempt to identify them as the manifestation of expanding gas resulting from a variety of mechanisms. Typically, these kinematic components have been associated with expanding shells, as in NGC 604 (Sabalisck et al. 1995) or 30 Doradus (Yang et al. 1996). More recently, Relaño & Beckman (2005; henceforth RB) analyzed complete samples of HII regions in NGC 1530, NGC 3359, and NGC 6951 using Fabry-Perot interferometry. They find broad kinematic components of low intensity and high velocity (henceforth, "wings") in a substantial fraction of these HII regions, which they interpret as due to an expanding shell within them. They compare the energetic properties of these HII regions with nearby examples such as NGC 604 and 30 Doradus. Among other issues, they consider whether these shells might arise as a result of the interaction between stellar winds and the interstellar medium.

Whether stellar winds sweep up shells that are themselves responsible for the features observed in line profiles of HII regions has a tangled history. Dyson (1979) modelled the supersonic widths of the line profiles in M33 and M101 (Smith & Weedman 1970; Melnick 1977) as the result of stellar winds. He considers the possibility that the OB associations within HII regions generate a shell of shocked gas that expands into the surrounding HII region, producing the observed supersonic velocities. Based upon assumed stellar parameters (luminosity, Lyman continuum flux, mass loss rates, and wind velocities), Dyson deduces the number of stars required to produce the observed line profiles and estimates the time scale during which the expanding shell is observable. The formation of this single shell as a result of the interaction of the shells formed by the winds of individual stars occurs almost instantly, since he explicitly assumes no spread in the turn-on times of the winds from individual stars. However a more sophisticated model by Dyson (1981), in which the winds originating from stars that

Send offprint requests to: M. Rozas

switch on later flow more rapidly until they impinge on the existing expanding shell, leads effectively to the same result and covers the case of a natural spread in the formation times of the stars in the cluster.His best-fitting models were those in which the expanding shell absorbed more than 50% of the UV flux from the central source. Since an unresolved, expanding shell produces a flat-topped line profile, Dyson (1979) postulated a background emission component for the HII regions whose turbulent motions did not exceed the sound speed in order to recover the gaussian line shapes observed.

Melnick (1980) rejected Dyson's (1979) model on the basis that the halo of NGC 604, a giant extragalactic HII region in M33, showed velocity dispersions exceeding the sound speed, thereby contradicting Dyson's (1979) model if the halo is assumed to provide the background emission. Rosa & D'Odorico (1982), on the other hand, undertook a detailed study of the kinematics of NGC 604, finding 12 structures having the shapes of shells with mean radii of approximately $r \sim 25$ pc and a mean expansion velocity of $v \sim 25\,\mathrm{km\,s^{-1}}$, characteristics that they deemed feasible through the action of stellar winds from 50 WR stars, each with a mass loss rate of $10^{-5} M_{\odot}\mathrm{yr}^{-1}$. Hippelein et al. (1986), who found a clear correlation between the H_{α} luminosity and velocity dispersion in 43 giant extragalactic HII regions (GEHRs), interpreted their result as evidence in favour of stellar winds, arguing that interactions between the shells swept up by the winds from individual stars dissipates a kinetic energy proportional to the number of massive stars with winds. Melnick et al. (1987) countered that the relation they obtain between the H_{β} luminosity and velocity dispersion based upon the assumption that stellar winds are responsible for the turbulent motions does not agree with the relation they observe. They argue that this result is due to the low efficiency with which the mechanical energy in winds is converted to kinetic energy in the ionized gas and to the lack of WR stars in some HII regions with supersonic velocity dispersions. Recent studies involving large numbers of HII regions continue to find supersonic line widths in HII regions, but have also found faint, high velocity kinematic components, denoted wings, in a substantial fraction of the brightest HII regions (Rozas et al. 1998, 2005, RB) and have interpreted these high velocity components as the kinematic signature of expanding shells powered by the winds of massive stars. If this last deduction is correct, the wind-blown shells postulated by Dyson (1979) may well have been found in GEHRs, though it may still not be clear that they serve the purpose originally intended.

As RB note, it is important to determine whether the presence of wings in the line profiles is a general phenomenon. So far, there are few studies of this issue, primarily due to the observational difficulties of obtaining data with the required spatial and spectral resolution for HII regions beyond the Local Group. To address this issue, large samples of HII regions are required.

Here, we analyze the broad, low intensity kinematic components found in the line profiles of a sample of 43 bright, isolated HII regions in ten spiral galaxies for which we have photometric and spectroscopic data (NGC 157, NGC 925, NGC 3631, NGC 6764, NGC 3344, NGC 4321, NGC 5364, NGC 5055, NGC 5985, and NGC 7479). We confirm the presence of these kinematic components, which we denote "wings", in the majority of the sample (37 HII regions) and interpret them as the result of expanding shells within the HII regions. We compute the kinetic energy associated with these expanding shells and the energy input requirements to produce them for each HII region using representative physical parameters of the shells observed in nearby HII regions. We conclude that these wings might well result from the winds from the ionizing stars, provided that account is taken of the density-bounded nature of the brightest giant extragalactic HII regions (Rozas et al. 1996; Rozas et al. 1998; Beckman et al. 2000; Zurita et al. 2000).

2. The data

The global properties of the galaxies from which we extract our sample of HII regions as well as a description of the observations and data reduction are given in Rozas et al. (2005; henceforth paper I). Here, we simply note that our sample of HII regions was chosen from among the brightest and most isolated HII regions in each galaxy in order to secure the most reliable measurements of nebular radius and avoid problems with crowding. For details of the measurements, we refer the reader to paper I.

As noted in paper I, the line profiles normally contain three kinematic components: a bright, central component and two roughly symmetric fainter components displaced to higher (absolute) velocities. In only one case (of 43) does the profile contain two central components of similar intensity. In five additional cases, the profile was fit with a single gaussian component, there being no evidence of any wings. For the present analysis we ignore these six deviant cases, since our purpose is to study the profiles with wings. It is useful to point out here that the relatively complex procedure for deconvolving the instrument function described in RB for their Fabry-Perot observations was not required when reducing the present data, since the response function of our slit spectrograph was well behaved and did not have high level extended wings.

3. The wing features

In paper I (Fig. 1), we present examples of these wings. These wings are kinematic components displaced, approximately symmetrically, about the brighter, central component. A more detailed study of the central high intensity components including considerations of the possible sources of broadening of the central peak is presented in Paper I. The criteria we use to define these wings are

- The intensity of these features must be at least 2.5 times greater than the rms noise level of the line profile.
- These features must be separated from the bright, central component by at least 2.5 times the spectral resolution. In our case, this implies separation limits in velocity of 27.5 km/s.
- These features must have a velocity dispersion that exceeds the instrumental resolution of 11 km/s.

In order to determine the properties of the line wings, we adjust gaussian components to the line profiles extracted using

different apertures. To select the best fit, we consider two parameters: the mean signal-to-noise ratio of the two components and the mean relative error of the standard deviation of the Gaussian fitted to both wings. In 94% of the cases, these two criteria coincide. We select the parameters from the fit with the best signal-to-noise to characterize the properties of the wings. We study the wing features through their physical properties: the fractional flux, velocity shift, and velocity dispersion of the blue and red wings, respectively.

We take the fractional flux as proportional to the Emission Measures and the fractional Emission Measure of the wing features is obtained as the ratio between the wing area and the total area of the line profiles. These parameters are given in Table 1. The relations between the fractional emission measures, velocity shifts, and velocity dispersions as a function of the Hα luminosity for the HII regions in Table 1 are shown in Figs. 1-6. In these figures, the error bars plotted are the formal errors from the fitting routine.

Figs. 1 and 2 plot the fractional emission measure of the blue and red components, respectively, as a function of the logarithmic Hα luminosity of each region. In both figures, the corresponding linear fits to the data are also shown. From these fits, we can see that there is no clear variation of the fractional emission measure of the wings with the logarithmic Hα luminosity, a result that agrees with the findings of RB although, nominally, our fits to these relations show somewhat larger correlation coefficients: r_{blue} = -0.1641 and r_{red} =-0.2102, versus r_{blue} = -0.1007 and r_{red} = -0.1405 from RB. The mean error of the fractional EM obtained from the error of the component area given by the fitting routine is 3.2% and 3.4% for the blue and red wings, respectively. The mean fractional emission measures in the blue and red wings are identical, 13.82% and 13.78%, respectively. RB also find the same mean fractional emission measures in the blue and red wings, but they find that they each contain 8.9% of the total flux.

Figs. 3 and 4 plot the velocity separation between the blue and red wings and the bright, central component as a function of the logarithmic Hα luminosity. Again, both wings behave similarly, being displaced approximately symmetrically in velocity about the central kinematic component, the mean values being $< V_{blue} >=$ 67.6 km/s and $< V_{red} >=$ 66.5 km/s for the blue and red wings, respectively. The range of velocity separations is 45–80 km/s, slightly less than found by RB, who found separations up to 90 km/s. Like RB, we find that there is a slight trend of increasing velocity separation with increasing luminosity, though this is more evident in the present case. This trend can be seen in the linear fits plotted for each parameter with linear correlation coefficients r_{blue} = 0.5009 and r_{red} = 0.4443 for the blue and red wings, respectively. The mean error in the velocity separation of the blue and red wings obtained from the fitting routine is 5.5 and 5.4 km/s, respectively, approximately the half of the spectral resolution of the data.

Figs. 5 and 6 plot the velocity dispersion of the red and blue wings, respectively, as a function of the logarithmic Hα luminosity. Once more, the results are similar for both wings, with the velocity dispersions spanning ranges of 18–35 km/s, though the slope of the relation for the blue wing is somewhat steeper than that for its red counterpart, as can be seen from comparison of the plots. There is a clear tendency for the velocity dispersions of the wings to increase with luminosity, which can be seen in the linear fits plotted for each parameter with linear correlation coefficients r_{blue} = 0.6878 and r_{red} = 0.6328 for the blue and red wings, respectively. The mean velocity dispersions we find for the blue and red wings are $< \sigma_{blue} >=$ 26.4 km/s and $< \sigma_{red} >=$ 27.5 km/s, respectively, well above the

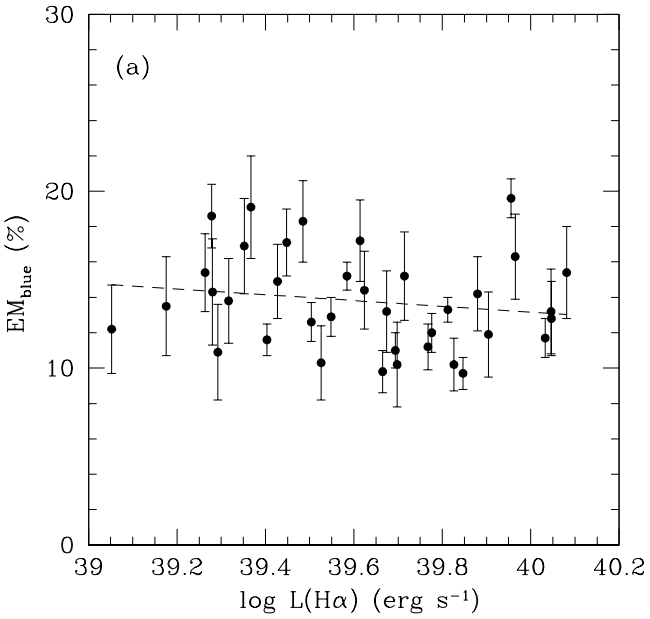

Fig. 1. The fractional emission measure of the blue wing as a function of the logarithm of the total Hα luminosity.

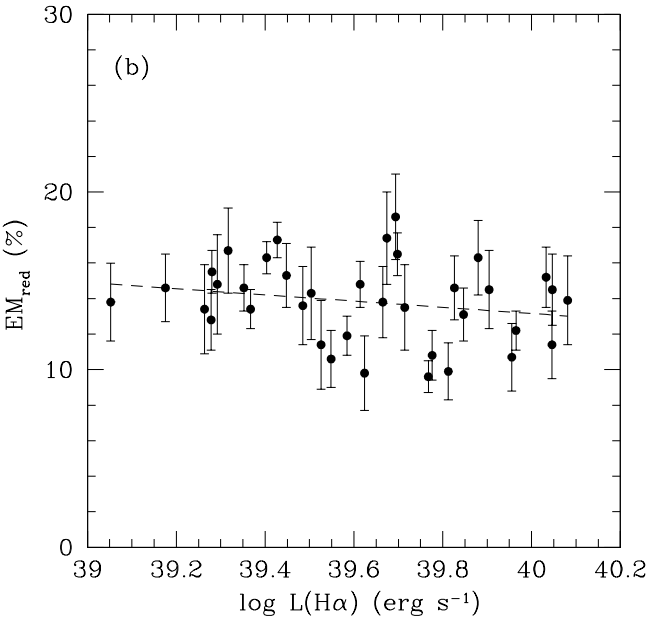

Fig. 2. The fractional emission measure of the red wing as a function of the logarithm of the total Hα luminosity.

Table 1. Wing parameters: column 1 - identification number and galaxy containing the HII region; column 2 - logarithm of the Hα flux; columns 3 and 4 - fractional emission measure in the blue and red wings; columns 5 and 6 - velocity shift of the blue and red wings; columns 7 and 8 - velocity dispersions of the blue and red wings.

Region (galaxy)	log Hα (erg s^{-1})	%EM$_b$ (pc cm^{-6})	%EM$_r$ (pc cm^{-6})	V$_b$ (km s^{-1})	V$_r$ (km s^{-1})	Δv_r (km s^{-1})	Δv_b (km s^{-1})
1 (NGC 925)	39.0525	12.2	13.8	45.6	51.1	21.2	22.0
2 (NGC 925)	39.1758	13.5	14.6	49.4	46.0	24.5	19.2
3 (NGC 925)	39.2638	17.1	15.3	59.1	59.5	28.0	25.9
4 (NGC 3631)	39.2785	15.4	13.4	53.3	45.3	24.1	21.1
5 (NGC 5364)	39.2804	14.3	15.5	62.2	57.1	25.7	25.3
6 (NGC 5364)	39.2924	18.6	12.8	50.1	57.3	22.6	18.9
7 (NGC 3631)	39.3167	16.9	14.6	47.6	53.1	28.8	22.8
8 (NGC 4321)	39.3521	10.9	14.8	57.3	64.5	24.0	24.3
9 (NGC 5055)	39.3674	13.8	16.7	70.3	65.0	24.3	26.1
10 (NGC 3631)	39.4036	19.1	13.4	65.8	70.2	26.5	28.0
11 (NGC 3344)	39.4276	11.6	16.3	75.2	68.6	24.3	20.1
12 (NGC 3631)	39.4482	18.3	13.6	77.2	65.1	29.7	27.2
13 (NGC 4321)	39.4848	14.9	17.3	64.0	67.2	27.1	24.4
14 (NGC 4321)	39.5036	12.6	14.3	68.4	70.3	24.6	33.1
15 (NGC 6764)	39.5258	10.3	11.4	80.5	73.2	28.2	22.2
16 (NGC 6764)	39.5486	12.9	10.6	63.5	60.4	31.1	27.4
18 (NGC 6764)	39.5845	15.2	11.9	59.1	68.4	32.8	27.8
21 (NGC 5364)	39.6138	17.2	14.8	75.1	79.2	29.1	26.0
22 (NGC 5055)	39.6237	9.8	13.8	53.2	65.3	32.6	28.3
23 (NGC 3344)	39.6652	10.2	16.5	69.2	62.7	27.9	20.9
24 (NGC 5985)	39.6743	11.0	18.6	66.5	60.2	32.4	27.2
25 (NGC 5985)	39.6940	13.2	17.4	49.6	58.0	28.0	23.7
26 (NGC 157)	39.6982	14.4	9.8	64.8	76.1	29.4	27.5
27 (NGC 5055)	39.7145	15.2	13.5	58.8	77.9	24.5	25.8
29 (NGC 157)	39.7675	11.2	9.6	69.9	78.8	23.6	23.7
30 (NGC 5055)	39.7764	12.0	10.8	72.2	70.1	29.1	22.2
32 (NGC 5985)	39.8126	13.3	9.9	71.0	63.7	25.8	33.1
33 (NGC 7479)	39.8265	10.2	14.6	65.1	60.2	33.6	26.4
34 (NGC 5985)	39.8469	9.7	13.1	69.2	72.1	28.4	27.0
36 (NGC 6764)	39.8796	14.2	16.3	76.7	67.9	27.6	30.9
37 (NGC 157)	39.9046	11.9	14.5	68.4	71.0	34.2	28.9
38(NGC 157)	39.9557	19.6	10.7	70.7	62.2	28.0	34.0
39 (NGC 7479)	39.9649	16.3	12.2	59.1	61.0	29.1	32.2
40 (NGC 7479)	40.0328	11.7	15.2	72.9	75.8	33.6	31.3
41 (NGC 7479)	40.0462	12.8	14.5	74.5	62.9	30.2	31.8
42 (NGC 157)	40.0468	13.2	11.4	66.2	58.1	31.5	29.1
43 (NGC 157)	40.0815	15.4	13.9	69.4	72.2	28.3	32.9

instrumental resolution. These values are significantly larger than the velocity dispersions found by RB, a difference that is easily understood as resulting from our sample containing *only* the brightest HII regions whereas RB's sample included fainter objects. The mean errors of the best fit for the blue and red velocity dispersions obtained from the fitting routine are 3.4 and 3.2 km/s, respectively.

4. The shells

4.1. Comparison with nearby HII regions

Considering the size of the slit used for our observations and the HII regions in our sample (paper I), our kinematic data are approximately unresolved. In order to better interpret these data, we first review the results obtained for the two brightest nearby HII regions, NGC 604 and 30 Dor, whose luminosities overlap those of the objects in our sample. Both the kinematics of the HII regions as well as the properties of the ionizing clusters are important. Finally, we compare expectations with some theoretical models.

Rosa & D'Odorico (1982) find that NGC 604 is a very inhomogenous object, composed of various expanding shells. They attribute this structure to the presence of winds from $\sim$ 50 WR stars. Melnick (1980) then observed gaussian profiles due to the large aperture that he used, thereby averaging the line profile over various unresolved structures. Subsequently, Rosa & Solf (1984) further studied NGC 604's velocity field, resolving what had been considered gaussian profiles into multiple components and finding asymmetries in the surface brightnesses of blue and red components along the line of sight. Furthermore, they found evidence for cavities and shells near the positions of luminous WR stars. These properties lead them to propose a

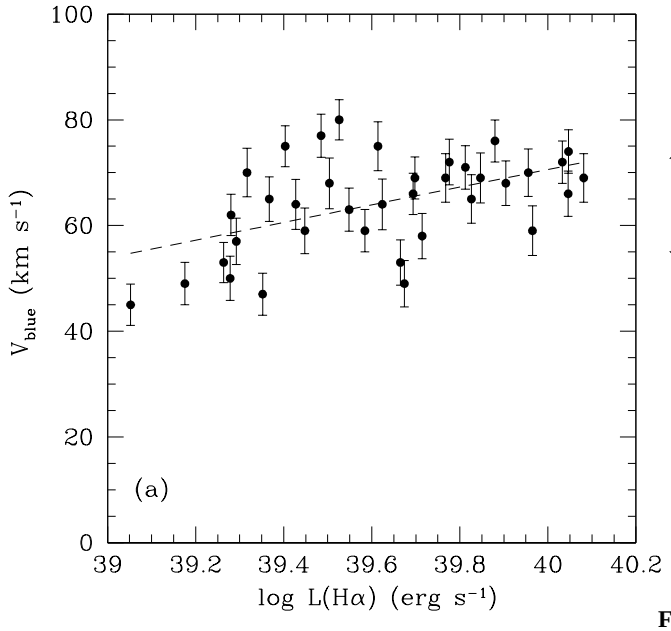

Fig. 3. The velocity separation of the blue wing from the bright, central component as a function of the logarithm of the total Hα luminosity.

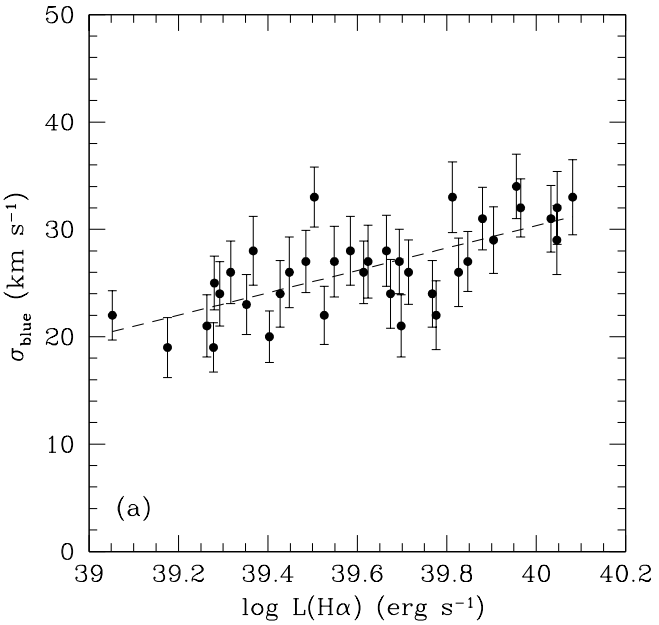

Fig. 5. The velocity dispersion of the blue wing as a function of the logarithm of the total Hα luminosity.

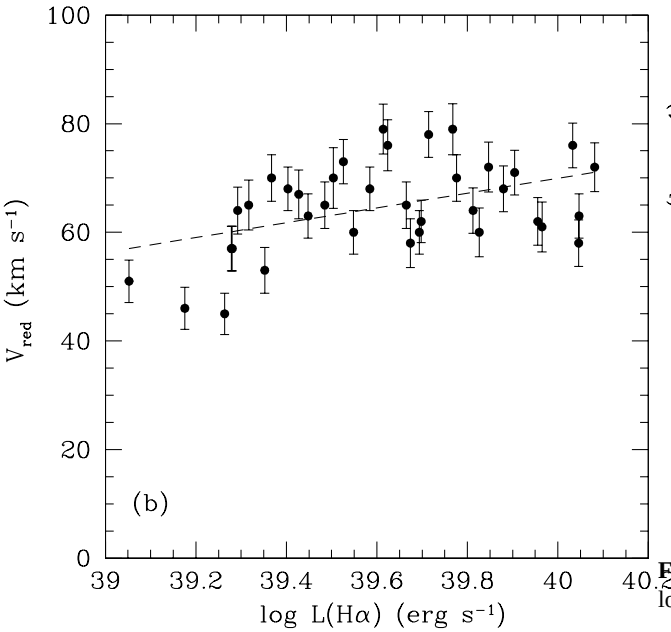

Fig. 4. The velocity separation of the red wing from the bright, central component as a function of the logarithm of the total Hα luminosity.

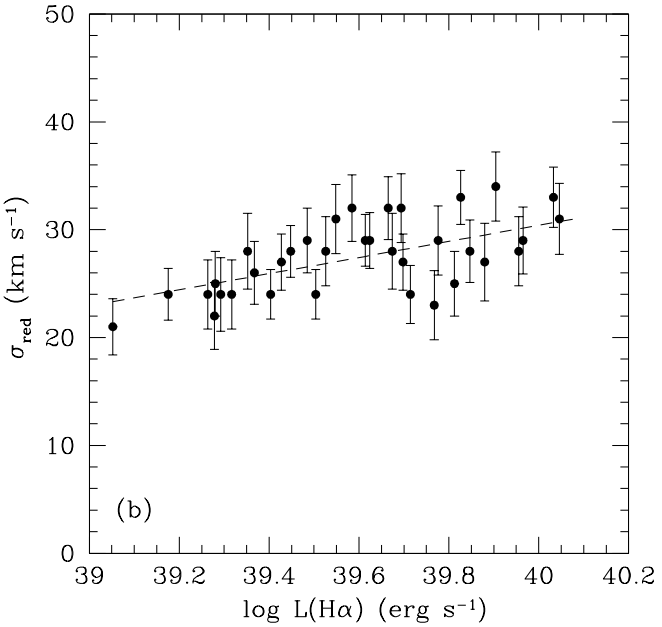

Fig. 6. The velocity dispersion of the red wing as a function of the logarithm of the total Hα luminosity.

blister structure for NGC 604 in which expanding shells due to the winds of WR stars were important, but not the only mechanism in explaining the kinematics of such an inhomogeneous region as NGC 604.

Chu & Kennicutt (1994) studied the internal kinematics of 30 Dor in the LMC. Although the outer regions of 30 Dor are dominated by a velocity field with a velocity dispersion $\sigma \sim 15 - 20\,\mathrm{km\,s^{-1}}$, they detect different velocity structures in the inner regions associated with expanding shells of different sizes and covering a range of velocities. While the slowly expanding shells are associated with bubbles blown by the winds of individual stars or small OB associations, the most rapidly expanding shells could be due to supernova explosions. The integrated line profile of the entire region may be fit with a broad gaussian with low intensity wings. Chu & Kennicutt (1994) reject the idea that the kinematics in the core could be due to gravitational effects, and suggest that the gaussian shape and velocity dispersion of the integrated profile is the result of the

superposition of individual expanding shells formed by stellar winds as well as champagne flows and possibly supernova remnants.

For 30 Dor, the synthetic profiles obtained by Tenorio-Tagle et al. (1996) that reproduce the integrated velocity dispersion in the core of this nebula imply shells with supersonic expansion velocities. They postulate that these supersonic velocities are due to low energy stellar winds from low mass stars that are moving supersonically in the gravitational potential of the entire system. The motions of the sources and the shocks due to their winds produce velocity dispersions in the medium such that $\sigma_{gas} \sim \sigma_{stars}$, but that the unresolved shells are disrupted before being slowed by the interstellar medium to subsonic velocities.

A careful inspection of our line profiles reveals not only the supersonic central component considered by Dyson (1979), but also much wider wings. It is these wings that provide what could be interpreted as direct evidence of the effects of winds, and it is possible that this phenomenon contributes to the general turbulence when the energy is dissipated. As discussed by RB, the assumption of a single expanding shell may appear arbitrary and a dramatic simplification of the results found in detailed studies of nearby, bright HII regions, such as 30 Doradus and NGC 604, where multiple shells are observed at different radii, but, in fact, even in these objects, one of the shells is by far the brighter and, in both cases, has a radius of about 20% of the HII region radius. In the case of NGC 604, the luminosity of this shell, with an expansion velocity of almost 70 km s^{-1}, represents 75% of the total luminosities of all of the shells observed. In the case of 30 Doradus, Melnick et al. (1999) fit the line profile reported by Chu & Kennicutt (1994) with two gaussian components with widths of σ = 22 km s^{-1} and σ = 44 km s^{-1}. The second, broader, component could be interpreted as an expanding shell observed with velocity resolution or signal-to-noise too low to resolve it into wings similar to those found for our sample. This might explain why the line profile obtained by Smith & Weedman (1972) via Fabry-Perot interferometry for this object shows two peaks separated by 45 km s^{-1} since Fabry-Perot interferometry is sensitive to low intensity components that cover a significant fraction of the projected area of the HII region. We therefore wonder whether the shells we infer from the line profiles for our sample of HII regions might not be similar to the expanding shells seen in these nearby, bright HII regions. Likewise, we see no reason to deny that multiple shells might be present in the HII regions in our sample, as there are in these two well-studied, nearby cases, but their presence would be difficult to discern in our line profiles.

Whether stellar winds or supernova explosions should dominate the injection of mechanical energy depends upon the ages of the embedded clusters. Certainly, once supernova explosions begin to occur, they will quickly dominate the mechanical energy budget (Leitherer et al. 1999). On the other hand, this will not occur too rapidly as the coupling factors for this input are not high, as we will discuss below. A recent study of the stellar content of NGC 604 suggests that the ionizing cluster is very young, $\sim$ 3 Myr, and represents a reasonably instantaneous burst of star formation (González & Pérez 2000). Their models predict between 150 and 215 O stars, including very massive ones whose ionizing radiation alone is sufficient to ionize the nebula. They predict that few ionizing photons should escape the region. They also conclude that stellar winds supply sufficient energy to form the central shell that is observed in the core of the cluster. Bruhweiler et al. (2003) confirm the youth of the stellar cluster and the presence of very massive stars. Meanwhile, Maíz-Apellániz et al. (2004) agree that the cluster is very young, but also forcefully argue that the nebula is optically thin over an entire quadrant and is leaking ionizing photons. Summarizing, there is a broad consensus that the cluster is very young. Considering STARBURST99 models, a cluster as young as 3 Myr should not yet have produced significant numbers of supernovae, for either instantaneous or continuous modes of star formation.

As regards 30 Doradus, Scowen et al. (1998) find that the ionizing radiation and stellar winds emitted by the central cluster are sufficient to explain the structure observed. Their principal conclusion is that its structure and characteristics are probably typical of giant extragalactic HII regions, though the example of Chen et al. (2005) would dispute this. Bosch et al. (2001) studied the star formation history in 30 Doradus and found three bursts of star formation with ages 5 Myr, 2.5 Myr, and $<$ 1.5 Myr, without much evidence of spatial segregation with age. As with NGC 604, it would appear that stellar winds should be a greater source of mechanical energy input than are supernovae.

Going further afield, the clusters in the brightest HII regions in M101 and NGC 2403 also appear to be young. Drissen et al. (1999) find that the ionizing clusters in four of the six brightest HII regions in NGC 2403 are younger than 7 Myr and possibly as young as 2 Myr. (They did not observe the third brightest HII region and do not present an age for the cluster in the sixth brightest.) The luminosities of these six HII regions overlap the range of luminosities considered here. They do note, however, the presence of older stars in the same regions surrounding these HII regions. Likewise, Chen et al. (2005) find that there is an abundance of clusters younger than 5 Myr in NGC 5461, NGC 5462, and NGC 5471, all in M101 and within the range of luminosities in our sample, but that older stars are also present. Clearly, young clusters appear to be common in giant extragalactic HII regions, but they are also not the only stellar population present.

The STARBURST99 models of Leitherer et al. (1999) provide further guidance. For instantaneous star formation, bright HII regions require young star clusters to provide the ionizing radiation observed. For either instantaneous or continuous star formation scenarios, the energy input from supernovae becomes so large by about 10 Myr that it exceeds the kinetic energy observed in the HII region, E_{turb} (Sect. 4.2; Table 2), by at least order of magnitude and it is questionable whether this would not disrupt the HII region entirely, even if 90% of this mechanical energy were dissipated either radiatively or in turbulence (e.g., Thornton et al. 1998). These considerations argue that the stellar clusters in the brightest HII regions will typically be young. Consequently, stellar winds are expected to be the dominant source of mechanical energy. A dynamical point to consider is that although the energy supply from SNe might appear to dominate the input to a shell after 10^7

years, this simple inference does not take into account the fact that the fraction of the available energy of a SN remnant that can be transferred to a massive shell already in much slower expansion depends on momentum balance rather than a simple energy balance. SNe inevitably occur after the stellar winds have already created a massive shell, sweeping out a volume of some tens of pc radius in the objects we are studying. This shell predictably has a mass of order a few $\times\, 10^4$ M$\odot$, based on rough values for the volumes and densities of the HII regions (and masses of this order are in fact observed in our shells, as shown in Table 2 below). The dynamical coupling of a SN remnant of mass 10 M$\odot$ and a velocity of order 10^4 km s^{-1} to an expanding shell of mass 10^4 M$\odot$ and a velocity $\lesssim$ 100 km s^{-1} is at most 10 %. One must take this factor into account before deriving the time at which the kinetic energy input to the shell due to SNe exceeds the integrated wind input. As the wind coupling has been estimated by Dyson (1980, 1981) to be $\sim$ 25 %, efficient, the time at which E(SN), the injected energy from supernovae, exceeds E (W) the injected energy from winds will be enhanced by a factor of at least 2 compared with the value which would be derived by simply calculating the overall rates of energy production by the two processes, using a standard code, such as Starburst99. These considerations strengthen our view that in the relatively young HII regions we observe most of the shell kinetic energy was injected by winds, although for older regions with shells of even larger radii, the contributions by SNe will tend to become more important.

4.2. Physical parameters

Following the inference of RB, we shall interpret the wings we find in our line profiles as the result of an expanding shell within the HII regions. This is reasonable given the very similar properties of the blue and red wings in individual HII regions, which implies that they arise from a single structure. In this case, we interpret the main emission component as coming from the bulk of the HII region while the expanding shell produces kinematic components symmetric about the main component, but of lower luminosity and higher velocity. Based upon the observed parameters for the wings and the properties of the principal shells in NGC 604 and 30 Dor, we intend to derive the density and energy of the shell.

If we suppose that the shells are completely ionized with a thickness ΔR_{shell}, their Hα luminosities may be expressed as

$$L(H\alpha)_{shell} = 4\pi R^2_{shell} \Delta R_{shell} n^2_{shell} h\nu_{H\alpha} \alpha^{eff}_{H\alpha}(H_0, T) \qquad (1)$$

where R_{shell} and n_{shell} are the radius and electron density of the (ionized) shell, respectively, h is Planck's constant, while $\nu_{H\alpha}$ and $\alpha^{eff}_{H\alpha}(H^\circ, T)$ are the frequency and the effective recombination coefficient for Hα, respectively.

We can use Eq. 1 to estimate the electron density of the shell if we assume values for the radius and thickness of the shell and if we suppose that the Hα luminosity of the shell represents the fraction of the total luminosity for the HII region corresponding to the fraction of the flux in the wings of the line profile. We shall adopt the same values of R_{shell} and ΔR_{shell} as RB, namely $R_{shell} = 0.2R_{reg}$, where R_{reg} is the radius of the HII region, and $\Delta R_{shell} = 4.5$ pc. As discussed above, the choice of these values is motivated by the examples of NGC 604 and 30 Dor.

The resulting values for the electron densities are given in column 3 of Table 2. In Table 2, we also include the mean expansion velocity, for which we adopt the mean of the relative velocity of the blue and red wings with respect to the central kinematic component. Likewise, Table 2 includes the adopted shell volume.

Given the radius of the ionized shell and its electron density, we compute the shell's mass according to

$$M_{shell}(H^+) = (1 + Y)\, 4\pi R^2_{shell} \times \Delta R_{shell} \times n_{shell} \times m_p \qquad (2)$$

where Y is the helium mass fraction, for which we adopt 0.25, and m_p is the mass of atomic hydrogen. These masses are tabulated in column 5 of Table 2. The shell masses are of order 10^5 M$_\odot$, typically an order of magnitude larger than found by RB. This is due to our selection of HII regions that are in general more luminous than those in RB; where the luminosities overlap the shell masses also coincide. Our shell masses represent less than 10 % of the total computed masses of the HII regions, a rather smaller fraction than that found by RB, which again could be due to the difference in the range of our selected HII region luminosities.

We can now use this mass to calculate the kinetic energy of the shells, $K = 1/2 m_{shell} v^2_{shell}$, in order to compare this with the energy emitted by the ionizing stars. This kinetic energy appears in column 6 of Table 2 and ranges from 1.8 to 12.5 $\times$ 10^{51} erg.

The wind energies from the ionizing stars were estimated based upon the luminosity in Hα for the HII regions. From this luminosity, the number of O3(V) stars required to provide it is deduced using the luminosities of these stars from Vacca et al. (1996). As suggested by RB, this number of O3(V) stars is really a lower limit when account is taken of the ionizing radiation that escapes HII regions that are density bounded (Beckman et al. 2000; Zurita et al. 2000). Also, recent estimates of the temperatures of O(V) stars might imply reductions of 0.1 dex in their luminosities (Martins et al. 2002), which would also result in an underestimate of the number of equivalent O3(V) stars here. To estimate the integrated wind energies from these stars, we assume a mean lifetime of 10^6 years and a wind luminosity of $L_{wind} = 10^{37.08}$ erg s^{-1} (Leitherer 1998). Given the discussion earlier (Sect. 4.1) regarding the age of the stellar clusters in bright HII regions, adopting a lifetime of 10^6 years is likely to underestimate the interval over which the ionizing stars contribute wind mechanical energy. The number of equivalent O3(V) stars and their integrated wind luminosities are given in columns 7 and 8, respectively, of Table 2. We compare the wind energies with the energy in ionizing radiation, which we estimate from the number of ionizing photons for O3(V) stars from Vacca et al. (1996), $N_{Lyman} = 7.4 \times 10^{49}$ photons s^{-1}. The energy in ionizing radiation is given in column 9 of Table 2 and is typically 2 orders of magnitude greater than the wind energies. For comparison, column 11 of Table 2 provides an approximation for the total radiative energy from the ionizing stars, supposing that these emit as black bodies

with an effective temperature of $T_{eff} = 51230$ K and have a radius of $R = 13.2\,R_{\odot}$ (Vacca et al. 1996).

Finally, in column 10 of Table 2, we tabulate the turbulent kinetic energy of the HII region. This quantity is calculated from the total mass of the HII region and the non-thermal velocity dispersion of the principal component of the line profile (paper I):

$$E_{turb} = 1/2 M_{reg} \sigma_{nt}^2 \, . \tag{3}$$

These turbulent kinetic energies range from 10^{52} erg to 10^{53} erg.

5. The energetics of the shells

5.1. Stellar winds

The winds of stars of type WR, OB, Of, or LBV can be a decisive factor in the kinematics of some normal HII regions. In some cases, the interaction of these stars with the surrounding medium through their winds, mass ejections, and radiation can lead to the formation of ring nebulae (Chu; 1981). These stars may suffer mass loss rates of up to $10^{-5}\,M_{\odot}$ year^{-1} in the form of winds whose velocities range up to thousands of km/s. At the same time, these stars may emit 2 orders of magnitude more energy in the form of photons than the mechanical energy in their winds. Nonetheless, the effects of both forms of energy may be comparable, since the conversion efficiency of UV photons into kinetic energy is less than 1% while the conversion efficiency of mechanical energy into kinetic energy may be up to 20% (Dyson & Williams 1980). According to the Dyson & Williams (1980) model, the winds from the ionizing stars, whose motions greatly exceed the sound speed in the surrounding medium, produce shock waves in the surrounding medium that are braked only slowly. As a result of this interaction, a narrow shell is formed whose kinetic energy may be related to the wind luminosity according to

$$\kappa = 15/77 \dot{E_w} t \tag{4}$$

where $\dot{E_w} = 1/2 \dot{M_w} v_w^2$ and t is the mean lifetime of the ionizing stars. In this model, we should find a ratio of 0.2 between the kinetic energy of the shell and the wind luminosity, if the kinetic energy of the shells is a result of stellar winds. Figure 7 shows the ratio of the kinetic energy of the shells and the wind luminosity as a function of the Hα luminosity for the HII regions in our sample.

The ratio of the kinetic energy of the shells to the mechanical energy of the stellar winds is generally between 0.2 and 0.4, slightly higher than predicted theoretically. RB obtained a similar discrepancy. A variety of factors could contribute to this discrepancy. It is clear in Eq. 1 that the quantity $R_{shell}^2 \Delta R_{shell} n_{shell}^2$ is fixed by the shell's Hα luminosity. However, the quantity that figures in the calculation of the shell mass, Eq. 2, is $R_{shell}^2 \Delta R_{shell} n_{shell}$. In terms of the observables

$$M_{shell}(H^+) = \frac{L(H\alpha)_{shell}}{h\nu_{\alpha}\alpha_{H\alpha}^{eff}} \frac{m_p}{n_{shell}} \, . \tag{5}$$

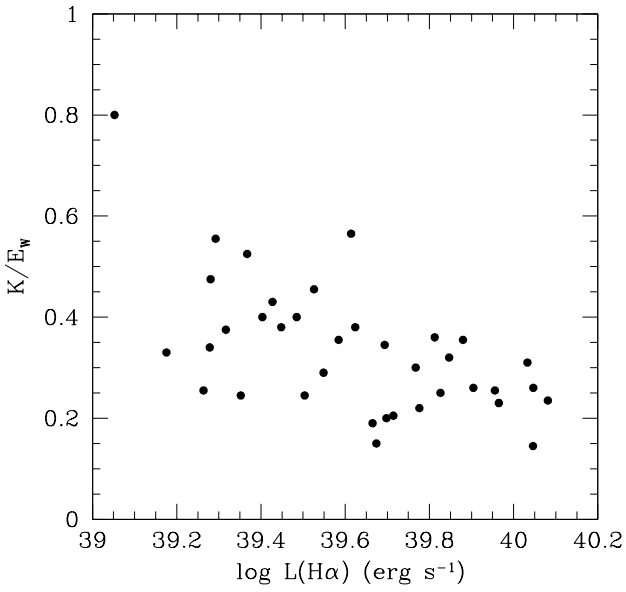

Fig. 7. The ratio of the kinetic energy of the shells and the energy in stellar winds as a function of the Hα luminosity, supposing shells with $R_{shell} = 0.2 R_{reg}$.

Therefore, the shell mass is not uniquely determined from the observations, though the densities adopted are motivated by the structure of shells observed in NGC 604 and 30 Dor, as discussed in Sect. 4.1. At present, we see no way of addressing this issue. We noted above that the time scale for the injection of wind mechanical energy has probably been underestimated, but our choice of the coupling efficiency from the models of Dyson & Williams (1980) is among the larger values found, so this may well compensate. Likewise, there are good reasons for supposing that the number of ionizing stars has also been underestimated for reasons already given (also see Sect. 5.2 below). At any rate, it is clear that there are significant uncertainties in calculating both the mechanical energy from stellar winds and the kinetic energy of the shell, so it is probably not surprising that the values are not in precise accord with theoretical expectations.

It is important to mention that RB carefully studied two of the most luminous HII regions in their sample and found that the shells might easily extend beyond $R_{shell} = 0.2 R_{reg}$ to $R_{shell} = 0.5 R_{reg}$. Considering that all of the HII regions in our sample are at least as bright as those in the sample of RB, it would perhaps be sensible to consider the possibility of $R_{shell} = 0.5 R_{reg}$ for our sample, its implications for the shell kinetic energy, and the latter quantity's ratio to the wind mechanical energy. In this case, the shell radius in Eq. 1 is increased by a factor of 2.5, leading to a decrease by the same factor in the shell density. From Eq. 2, this leads to an increase in the shell mass by the same factor of 2.5. This change would exaggerate the discrepancy with Dyson & Williams' (1980) result, leading to ratios of the kinetic energy of the shell relative to the wind mechanical energy as high as unity, values that would be impossible to explain as a result of stellar winds alone.

5.2. Matter-bounded HII regions

A variety of studies indicate that the brightest giant HII regions are matter-bounded, rather than radiation-bounded, i.e., the molecular cloud surrounding the ionizing stars is not sufficiently massive to absorb all of the ionizing radiation. In this case, some fraction of the ionizing radiation escapes from the HII region. McCall et al. (1985) studied a sample of 99 HII regions in 20 galaxies and found high [O III]λ5007/[O II]λ3727 ratios accompanied by small Hβ equivalent widths. They invoked matter-bounded HII regions to explain this result. Oey & Kennicutt (1998) use models of stellar atmospheres to predict the Hα luminosities of HII regions in the LMC based upon studies of their stellar content. Comparing these predicted Hα luminosities with those observed, they find that up to 51% of the ionizing radiation escapes the HII regions. and emphasise the existence of several HII regions which appear to be convincingly density-bounded. Our own studies of the luminosity functions of HII regions reveal a change in slope around an Hα luminosity of $10^{38.6}$ erg s^{-1}, which may be explained if the most luminous HII regions are matter-bounded (Rozas et al. 1996). The upper envelope of the $L - \sigma$ relation for HII regions in M100 may also be explained in terms of matter-bounding of the most luminous HII regions (Rozas et al. 1998). Beckman et al. (2000) explain the transition between ionization- and matter-bounded HII regions using a theoretical model that relates the mass of stars to the mass of the molecular cloud from which they form. Finally, Zurita et al. (2001) propose that photons escaping from matter-bounded HII regions are responsible for producing the diffuse ionized gas in galaxies, and conclude that up to 80% of ionizing photons might escape from HII regions into the diffuse medium. Finally, Maíz-Apellániz et al. (2004) claim to observe matter bounding directly in the case of NGC 604.

In column 2 of Table 3, we tabulate the ratio of the kinetic energy of the shells to the mechanical energy of the winds, supposing $R_{shell} = 0.5R_{reg}$. In column 3, we calculate the wind mechanical energy required from the ionizing stars to maintain compatibility with Dyson's (1979) model. From these data, we can calculate the number of ionizing stars that would be needed to make up the deficit of wind mechanical energy and the Hα luminosity that should be observed from the HII region were it not matter-bounded (keeping in mind the uncertainties noted earlier). These data are listed in columns 4 and 5. In column 6, we compute the percentage of ionizing radiation that is absorbed by the HII region, supposing it is matter-bounded and contains sufficient ionizing stars to explain the wind energies necessary to produce the shell kinetic energies.

The fraction of ionizing radiation that escapes the HII regions in Table 3 ranges from 45% to 90% with a mean value of 70%. These values are in good agreement with those deduced by Zurita et al. (2001), who propose that this escaping radiation is responsible for ionizing the diffuse ionized gas. Based upon the model of Beckman et al. (2000), they compute that up to 90% of the ionizing radiation escapes from the brightest HII regions. If this is the case, the stellar winds from the ionizing stars may provide more than sufficient energy to produce the shells that would be responsible for the wings seen in the line profiles of giant HII regions.

While it may be possible to explain the kinetic energy of the expanding shells as a result of stellar winds, it is clear that stellar winds will generally be unable to explain the turbulent motions observed in these HII regions. If 20% of the mechanical energy is used to power expanding shells, at most 80% is available to contribute to the generation of turbulent motions. For stellar winds to explain the turbulent kinetic energy, E_{turb}, the ratio E_{turb}/E_{wind} in Table 2 should be less than 4. Typically, this ratio exceeds 5 for the lower luminosity HII regions in Table 2 while it almost always exceeds 15 for the brightest HII regions. Increasing the stellar wind energies by a factor of 2.5 to account for the kinetic energies observed in the expanding shells, they are still insufficient to explain the turbulent energies in the brightest HII regions. Even if the conversion efficiency from wind to shell kinetic energy is lower, the additional energy available for conversion to turbulent kinetic energy is at most only 25% greater and so will still fall short for the brightest HII regions. Therefore, stellar winds would not appear to be a promising means to account for the turbulent energies observed in the brightest HII regions, though they may represent a dominant contribution for lower luminosity HII regions. The modelling situation here can be significantly improved by including the contribution from SNe since we know that less than 10% of the SN remnant energy can be taken up by the dominant expanding shell. Thus over 90 % of this kinetic energy is either radiated away or converted into turbulent motion in the main body of the HII region. Without a convincing detailed model we would not wish to speculate further here about the origin of the observed turbulence (paper I).

6. Conclusions

- We have studied the Hα emission line profiles of a sample of HII regions in 10 galaxies. The sample was chosen to include the brightest and most isolated HII regions in these galaxies. The majority (37 of 43 analyzed) have line profiles with wings of low intensity and high velocity. For the brightest HII regions, we therefore confirm the hypothesis advanced by RB that such wings are probably a general feature of HII regions.
- To determine the characteristics of these wings, we have fit them with gaussian components. The best fit was chosen considering the mean signal-to-noise of both components and the mean relative error of the standard deviation of the Gaussian fitted to both wings. To characterize these wings, we use the emission measures of the blue and red components, the fraction of the total emission measure for the entire HII region, and the velocity separation of the wings from the principal component.
- In individual HII regions, the blue and red wings are generally similar, with no large differences in their fractional emission measure, velocity separation from the main component, or internal velocity dispersion.
- The emission measure in the wings does not depend upon the total luminosity of the HII region. The average frac-

Table 2. Energies of the shell and turbulent components of the each HII region. Column 1 - identification number and galaxy containing the HII region. Column 2: Shell volumes. Column 3: Mean shell electron density. Column 4: Shell expansion velocity. Column 5: Ionized mass of the shell. Column 6: Kinetic energy of the shell. Column 7: Equivalent number of O3(V) stars. Column 8: Kinetic energy of OB stellar winds, assuming an equivalent number of O3(V) stars. Column 9: Energy of the ionizing radiation from the OB stars. Column 10: Turbulent kinetic energy of the HII region. Column 11: Total radiative energy of region OB stars emitting as black bodies.

Region (galaxy)	V_{shell} (10^3 pc^3)	n_{shell} (cm^{-3})	v_{shell} (km s^{-1})	M_{shell} (10^4 M$\odot$)	K (10^{51}erg)	N_{eq} (O3(V))	E_{wind} (10^{51} erg)	E_{rad} (10^{54} erg)	E_{turb} (10^{51} erg)	E_{TOT} (10^{54} erg)
1 (NGC 925)	190	31.06	48.3	14.4	3.4	11.01	4.17	0.57	5.31	1.44
2 (NGC 925)	310	10.56	47.7	8.0	1.9	14.62	5.54	0.76	7.62	1.91
3 (NGC 925)	184	16.45	59.3	7.4	2.6	17.92	6.79	0.94	15.14	2.34
4 (NGC 3631)	204	15.15	49.3	7.5	1.8	18.52	7.02	0.97	10.53	2.42
5 (NGC 5364)	293	13.26	59.6	9.5	3.4	18.61	7.05	0.97	11.11	2.43
6 (NGC 5364)	239	14.91	53.7	8.7	2.5	19.13	7.25	1.00	13.25	2.50
7 (NGC 3631)	165	18.58	50.3	7.5	1.9	20.23	7.67	1.06	10.72	2.65
8 (NGC 4321)	479	10.84	60.9	12.6	4.7	21.95	8.32	1.15	19.23	2.87
9 (NGC 5055)	141	20.80	67.6	7.2	3.3	22.73	8.61	1.19	10.99	2.97
10 (NGC 3631)	293	14.98	68.0	10.7	4.9	24.71	9.36	1.29	15.33	3.23
11 (NGC 3344)	165	19.30	71.9	7.8	4.0	26.12	9.90	1.37	14.21	3.41
12 (NGC 3631)	165	20.68	71.1	8.3	4.2	27.5	10.42	1.44	23.93	3.60
13 (NGC 4321)	254	18.38	65.6	11.4	4.9	29.79	11.29	1.56	20.13	3.90
14 (NGC 4321)	90	27.39	69.3	6.0	2.9	31.11	11.79	1.63	24.01	4.07
15 (NGC 6764)	318	12.54	76.8	9.7	5.7	32.74	12.41	1.71	25.69	4.28
16 (NGC 6764)	277	15.06	61.9	10.2	3.8	34.51	13.08	1.80	25.85	4.51
18 (NGC 6764)	277	18.64	63.7	12.6	5.1	37.48	14.21	1.96	38.00	4.90
21 (NGC 5364)	293	20.35	77.1	14.5	8.7	40.10	15.20	2.10	25.11	5.25
22 (NGC 5055)	141	24.73	59.2	8.5	3.0	41.02	15.52	2.15	48.33	5.37
23 (NGC 3344)	100	32.87	65.9	8.0	3.5	45.14	17.11	2.36	54.68	5.90
24 (NGC 5985)	362	17.26	63.3	15.2	6.1	46.10	17.47	2.41	33.17	6.03
25 (NGC 5985)	125	32.05	53.8	18.7	2.8	48.23	18.28	2.52	59.67	6.31
26 (NGC 157)	335	17.36	70.4	12.2	7.1	48.70	18.46	2.55	43.33	6.37
27 (NGC 5055)	141	29.54	68.3	8.5	4.0	50.56	19.16	2.64	71.29	6.61
29 (NGC 157)	239	20.25	74.3	11.8	6.5	57.12	21.65	3.00	64.26	7.47
30 (NGC 5055)	141	28.48	71.1	9.8	5.0	58.30	22.10	3.05	48.64	7.63
32 (NGC 5985)	521	15.20	67.3	19.3	8.8	63.38	24.03	3.32	68.42	8.29
33 (NGC 7479)	318	20.54	62.6	16.0	6.3	65.44	24.81	3.42	101.60	8.56
34 (NGC 5985)	390	17.63	70.6	16.8	8.4	68.60	26.01	3.59	84.01	8.98
36 (NGC 6764)	318	24.78	72.3	19.2	10.1	73.95	28.03	3.87	103.05	9.68
37 (NGC 157)	239	27.81	69.7	16.2	7.8	78.33	29.69	4.10	101.16	10.25
38 (NGC 157)	277	29.02	66.4	18.6	8.7	88.11	33.40	4.61	127.35	11.53
39 (NGC 7479)	362	24.74	60.0	21.8	7.8	89.01	33.74	4.66	138.39	11.65
40 (NGC 7479)	362	25.69	74.3	22.6	12.5	105.23	39.89	5.51	152.67	13.77
41 (NGC 7479)	344	27.13	68.7	22.7	10.7	108.52	41.14	5.68	127.67	14.20
42 (NGC 157)	177	36.43	62.1	15.8	6.1	108.67	41.20	5.69	153.38	14.22
43 (NGC 157)	239	36.40	70.8	21.2	10.6	117.71	44.62	6.16	96.61	15.46

tional emission measure in the blue and red wings is identical: ~ 14 % in both cases.

– The velocity separation from the main component is also similar for the blue and red wings. The range of velocity separations spans 45-80 km s^{-1}, with average values of $< V_{blue} >= 67.6$ km s^{-1} and $< V_{red} >= 66.5$ km s^{-1} for the blue and red wings, respectively. There is a tendency for the velocity separation to increase with increasing Hα luminosity.
– The internal velocity dispersions in the wings span a range of $18 - 35$ km s^{-1}. Although the relation between velocity dispersion and Hα luminosity is similar for the blue and red wings, the relation for the blue wing has a slightly larger slope. The mean velocity dispersions found are $< \sigma_{blue} >= 26.4$ km s^{-1} and $< \sigma_{red} >= 27.5$ km s^{-1}. There is a clear tendency for the velocity dispersions to increase with increasing Hα luminosity.
– Given the similar properties of the blue and red wings in individual HII regions, it seems natural to interpret them as arising from a coherent structure. We interpret these wings as evidence of expanding shells within the HII regions. We adopt the mean velocity of the blue and red wings as the expansion velocity of the expanding shell. Based upon comparisons with nearby extragalactic HII regions, we calculate the physical parameters and kinetic energies of these expanding shells.
– We compare the kinetic energies of the shells with the mechanical energies expected from the ionizing stars, suppos-

Table 3. The stellar wind energies required if the line wings are due to stellar wind-powered expanding shells and the fraction of ionizing luminosity observed, supposing the HII regions to be matter-bounded and that $R_{shell} = 0.5\ R_{reg}$. Column 1: Identification number of the HII region and the galaxy to which it belongs. Column 2: Ratio of the shell kinetic energy and the stellar wind energy provided by the number of equivalent O3V stars required to provide the observed luminosity. Column 3: The stellar wind energy required to bring the energy ratio in column 2 to its theoretical value of 0.2. Column 4: The number of equivalent O3V stars required to provide the wind energy in column 3. Column 5: The logarithm of the Hα luminosity that would be observed from an ionization-bounded HII region ionized by the number of equivalent O3V stars in column 4. Column 6: The percentage of the luminosity observed in each HII region.

Region (galaxy)	K/E_{wind}	E^*_{wind} (10^{51}erg)	N^*_{eq} (O3(V))	log $L^*(H\alpha)$ (erg s^{-1})	(100 – % L_{esc})
1 (NGC 925)	2.00	42.50	112.09	40.05	10.00
2 (NGC 925)	0.82	23.75	62.64	39.80	23.75
3 (NGC 925)	0.95	32.50	85.71	39.94	21.00
4 (NGC 3631)	0.63	22.50	59.34	39.78	31.51
5 (NGC 5364)	1.18	42.50	112.09	40.05	17.00
6 (NGC 5364)	0.85	31.25	82.42	39.92	23.55
7 (NGC 3631)	0.61	23.75	62.64	39.80	32.50
8 (NGC 4321)	1.38	58.75	154.82	40.19	14.50
9 (NGC 5055)	0.93	41.25	108.60	40.04	21.00
10 (NGC 3631)	1.31	61.25	161.41	40.22	15.20
11 (NGC 3344)	1.00	50.00	131.87	40.13	19.50
12 (NGC 3631)	1.00	52.50	138.46	40.15	19.50
13 (NGC 4321)	1.07	61.25	161.41	40.21	18.70
14 (NGC 4321)	0.61	36.25	95.47	39.99	32.50
15 (NGC 6764)	1.13	71.25	187.80	40.28	17.40
16 (NGC 6764)	0.72	47.50	125.28	40.11	27.00
18 (NGC 6764)	0.88	63.75	168.14	40.23	22.50
21 (NGC 5364)	1.41	108.75	286.70	40.46	14.20
22 (NGC 5055)	0.47	37.50	98.90	40.00	41.80
23 (NGC 3344)	0.50	43.75	115.30	40.06	40.00
24 (NGC 5985)	0.86	76.25	201.50	40.31	23.00
25 (NGC 5985)	0.38	35.00	92.31	39.97	52.60
26 (NGC 157)	0.95	88.75	234.40	40.37	21.00
27 (NGC 5055)	0.51	50.00	131.87	40.13	38.20
29 (NGC 157)	0.75	81.25	214.29	40.34	26.40
30 (NGC 5055)	0.55	62.50	164.84	40.22	35.50
32 (NGC 5985)	0.90	110.00	290.10	40.47	22.00
33 (NGC 7479)	0.63	78.75	207.70	40.32	31.70
34 (NGC 5985)	0.80	105.00	276.90	40.45	24.60
36 (NGC 6764)	0.88	126.25	332.85	40.53	22.00
37 (NGC 157)	0.65	97.50	257.15	40.42	30.30
38 (NGC 157)	0.63	108.75	286.70	40.46	31.00
39 (NGC 7479)	0.57	97.50	257.15	40.42	34.70
40 (NGC 7479)	0.77	156.25	412.10	40.62	25.80
41 (NGC 7479)	0.65	133.75	352.60	40.56	30.50
42 (NGC 157)	0.36	76.25	200.00	40.31	53.80
43 (NGC 157)	0.58	132.50	349.40	40.55	34.00

ing a number of stars sufficient to produce the Hα luminosity. The ratio of these energies is typically found to be between 0.2 and 0.4, slightly above the ratios predicted theoretically, supposing a shell radius 20% that of the HII region. This discrepancy is, perhaps, within the uncertainties in the calculation of the wind energies. On the other hand, the shells may well extend to 50-60% of the radius of the HII region, in which case it would be difficult to attribute the kinetic energy of the shells to the energy injected exclusively by stellar winds and although for these larger shells a dynamical contribution from SNe will be of some relevance, the relatively inefficient dynamical coupling here limits the energy that they can inject into the major shell, so that the observed shell kinetic energies are unlikely to have been produced principally by SNe.

– If we allow that the brightest HII regions may be matter-bounded, the above difficulty disappears. We compute the wind mechanical energy required to produce the shell kinetic energy according to Dyson & Williams' (1980) theory and compute the predicted Hα luminosity supposing the HII region to be ionization-bounded. Comparing these predicted Hα luminosities with those observed implies that between 45% and 90% of ionizing photons escape these very bright HII regions, a fraction in agreement with a va-

riety of other studies. If this is the case, stellar winds could provide the major part of the energy required to produce the wings seen in the emission line profiles from giant HII regions. However, for the brightest regions the subsequent injection of energy from SNe could well make an important contribution to the turbulent broadening of the main emission components observed in the regions.

– It appears improbable that stellar winds can inject the kinetic energy necessary to explain the turbulent motions observed in the brightest HII regions, but they may be the dominant contributors in lower luminosity HII regions.

Acknowledgements. MGR and JAL acknowledge financial support from CONACyT grant 43121-E as well as DGAPA grants IN112103, IN108406, and IN108506. We acknowledge the work of G. Melgoza and S. Monrroy as telescope operators during the acquisition of these data.

References

Arsenault, R., Roy, J. R. 1986, AJ, 92, 567
Beckman,J.E., Rozas,M., Zurita,A., Watson,R.A., Knapen,J.H. 2000, AJ, 119, 2728
Bosch,G., Selman,F., Melnick,J., Terlevich,R. 2001, A&A, 380, 137
Chen, C.-H. R., Chu, Y.-H., & Johnson, K. E. 2005, ApJ, 619, 779
Chu, Y.-H. 1981, ApJ, 249, 195
Chu, Y.-H., Kennicutt, R.C., 1994, ApJ, 425, 720
Drissen, L., Roy, J.-R., Moffat, A. F. J., & Shara, M. M. 1999, AJ, 117, 1249
Dyson, J. E. 1979, A&A, 73, 132
Dyson,J.E., Williams,D.A. 1980, Physics of the interstellar medium, ed. B.L.C. in Publication data (Manchester University Press)
Dyson J.E. 1981, in "Investigating the Universe", The dynamical effects of hypersonic stellar winds on interstellar gas, Ed. F. Kahn, Reidel, p. 125
Hippelein, H.H. 1986, A&A, 160, 374
Leitherer, C. 1998, Stellar Astrophysics for the Local Group, eds. Aparicio, A., Herrero, A., S?anchez, F. (Cambridge: Cambridge University Press), p. 527
Leitherer, C., Schaerer, D., Goldader, J. D., González Delgado, R. M., Robert, C., et al. 1999, ApJS, 123, 3
Maíz-Apellániz, J., Pérez, E., & Mas-Hesse, J. M. 2004, AJ, 128, 1196
Martins, F., Schaerer, D., Hillier, D. J. 2002, A&A, 382, 999
McCall, M.L., Rybski, P.M., Shields, G. A. 1985, ApJS, 57, 1
Melnick, J. 1970, ApJ, 213, 15
Melnick, J. 1980, A&A, 86, 304
Oey, M.S., Kennicutt, R.C. 1998, PASA, 15, 141
Relaño, M., Beckman, J.E. 2005, A&A , 430, 911
Rosa, M., D'odorico, S. 1982, A&A , 108, 339
Rosa, M., Solf, J. 1984, A&A, 130, 29
Rozas, M., Beckman, J. E., Knapen, J. H. 1996, A&A, 307, 735
Rozas, M., Sabalisck, N., Beckman, J. E., Knapen, J. H. 1998, A&A, 338, 15
Rozas, M., Richer, M. G., López, J. A. 2005, A&A, in press
Sabalisck, N., Tenorio-Tagle, G., Castañeda, H., Mu?nozTu?non, C. 1995, ApJ, 444, 200
Skillman, E., Balick, B. 1984, ApJ, 280, 580
Skillman, E. 1985, ApJ, 290, 449
Scowen,P.A., Hester,J.J., Sankrit,R., Gallagher,J.S., Ballester,G.E., Burrows,C.J., Clarke,J.T., Crisp,D., Evans,R.W., Griffiths,R.E., Hoessel,J.G., Holtzman,J.A., Krist,J., Mould,J.R., Stapelfeldt,K.R., Trauger,J.T., Watson,A.M., Westphal,J.A. 1998, AJ, 116, 163
Smith, M. G., & Weedman, D. W. 1970, ApJ, 161, 33
Tenorio-Tagle, G., Muñoz-Tunõn, C., Cid-Fernandes, R. 1996, ApJ, 456, 264
Thornton, K., Gaudlitz, M., Janka, H.-Th., & Steinmetz, M. 1998, ApJ, 500, 95
Vacca, W.D., Garmany, C. D., Shull, M. 1996, ApJ, 460, 914
Yang, H., Chu, Y. -H., Skillman, E. D., Terlevich, R. 1996, AJ, 112, 146
Zurita,A.; Rozas,M.; Beckman,J.E. 2000, A&A, 363, 9
Zurita, A., PhD. Thesis, Univ. La Laguna, 2001